Int. J. Multiphase Flow Vol. 17, No. 6, pp. 745–765, 1991
Printed in Great Britain.

0301-9322/91 $3.00 + 0.00

LIQUID AND GAS ENTRAINMENT TO A SMALL BREAK HOLE FROM A STRATIFIED TWO-PHASE REGION

T. YONOMOTO and K. TASAKA†
Department of Reactor Safety, Japan Atomic Energy Research Institute, Tokai, Ibaraki, 319-11, Japan

(Received 5 February 1990; in revised form 24 July 1991)

Abstract—A theoretical and experimental study has been conducted for liquid and gas entrainment to a small break hole from a stratified two-phase region. Theoretical correlations previously obtained for top, side and bottom entrainment were modified to express the relation between break flow rate, break quality and bulk water level so that they can be used easily for any break geometry. The modified correlations were assessed with experimental data obtained under room temperature and low pressure conditions using air and water. The experiment results were predicted well with the present model without using any adjustment coefficient when the upstream flow was symmetrical around the break. The effects of vortex, crossflow and wavy flow, observed in the experiment but not taken into account in the model, were empirically correlated based on the present correlation. By using the empirically modified correlations, the data in the literature, including high-pressure steam–water conditions, were reasonably predicted.

Key Words: entrainment, stratified flow, T-branch

1. INTRODUCTION

It is one of the most important issues in a safety study on a small break loss-of-coolant accident (LOCA) to accurately predict the flow rate through a small break hole at a cold or hot leg in a Westinghouse-type pressurized water reactor. Stratified flow tends to occur in large-diameter horizontal pipes, such as the hot and cold legs during a small break LOCA. This is because gravity is a dominant force in determining the hydraulics during this type of accident. The break quality is, therefore, significantly affected by an azimuthal location of the break on the pipe wall, as shown in figure 1. Liquid or gas entrainment play a dominant role in determining the break quality and flow rate.

Comparisons of the LOFT L2-5 small break LOCA test data and calculation results by LOCA analysis codes, such as RELAP5 and TRAC, made it clear for the first time that the flow rate through a small break on a horizontal pipe wall with stratified flow could not be predicted well by existing codes (Doa & Carpenter 1980). Zuber (1981) made an extensive survey of the literature and pointed out the lack of information relating to this problem. Since then several studies have been initiated. Reimann & Khan (1983) and Smoglie (1984; Smoglie & Reimann 1986) conducted air–water experiments for top, side and bottom oriented breaks, and presented detailed observational results. They made correlations for the break quality which were expressed as a function of h/h_b, a water level normalized by the onset water level for the entrainment. Experiments were conducted by Anderson & Owca (1985) for side and bottom oriented breaks with steam and water under pressure conditions of up to 6.3 MPa. Schrock *et al.* (1986) conducted experiments using both air–water and steam–water as working fluids. They concluded that the entrainment behavior was affected by differences in the physical properties and made the onset correlation for gas entrainment taking into account the physical property effects, including surface tension and viscosity. Their break quality correlation agreed well with the experimental data of Reimann and coworkers and Anderson & Owca (1985). Masiaszek & Memponteli (1986) performed experiments using steam and water under pressure conditions of up to 2.0 MPa. They obtained break quality correlations by assuming the break void fraction as a function of h/h_b and a slip ratio expressed with a square root of density ratio $\sqrt{\rho_L/\rho_G}$.

Several correlations have been obtained through the above studies, which have been derived mainly from dimensional analysis and empirical fitting with the experimental data. It should be

†Current address: Nagoya University, Nagoya, Aichi, Japan.

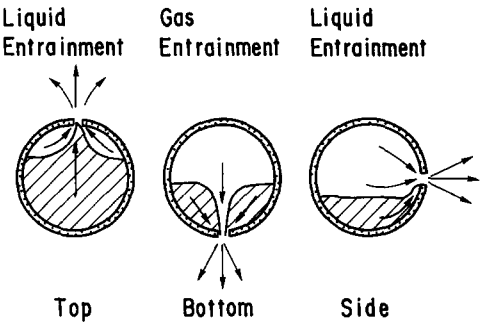

Figure 1. Break geometries.

noted that there is not an adequate physical model for the break quality even for a simple hydraulic condition. Therefore, in the present study the emphasis was primarily on the development of an analytical model based on physical understanding of the phenomena.

The authors' previous paper was concerned with the development of a physical model for the entrainment (Yonomoto & Tasaka 1988). A simple physical model was presented to analyze the entrainment, which assumed symmetrical flow upstream of the break. The break flow rate and quality were expressed as a function of density, and the single-phase gas and liquid flow rates which were calculated from the same pressure profile around the break as the two-phase flow condition in question. Experimental results were also presented which were attained using air and water under low pressure and room temperature conditions. Comparison of the results showed good agreement for the break quality and mass flux between the predictions and the experimental data without using any empirical constant for the liquid entrainment under symmetrical flow conditions in the upstream region. However, entrainment under more complicated hydraulic conditions was not studied in detail in that paper.

Although the applicability of the model to the LOCA condition had not been investigated in detail, this model was tentatively incorporated into the LOCA analysis code RELAP5/MOD2 (Asaka *et al.* 1990, 1991). The modified code was used for the analysis of the break orientation effects tests performed with the LSTF. The LSTF is a large-scale simulator of the pressurized water reactor used in the ROSA-IV program conducted by Japan Atomic Energy Research Institute. The prediction of the break flow rate was improved by using this model.

In this paper, we will present different mathematical expressions of the model in order to easily predict the break flow rate through any kind of break geometry. Experimental results will be presented concerning the effects of several hydraulic parameters on the entrainment behavior. The parameters include the vortex flow, crossflow etc. Then we will explain empirical modifications for the present model to take into account the parameter effects. Finally, a comparison will be made between the present correlations and the experimental data in the literature, which include the high pressure steam–water experiment results.

2. THEORY

2.1. Summary and additional discussions for the proposed model

A simple physical model for the liquid and gas entrainment from a stratified two-phase region into a small break hole has been developed (Yonomoto & Tasaka 1988). The coordination system of the model for the top break is shown in figure 2, where the liquid entrainment behavior is illustrated. The shape of the two-phase interface in the vicinity of the break has been predicted to be conical by the present model. A void fraction ϵ is defined as the ratio of the gas flow area to the hemispherical surface area in the conical surface region. The boundary r_m shown in figure 2 is defined by extrapolating the conical surface region so that it intersects the bulk water level. The boundary r_S shown in figure 2 is an imaginary boundary between a smooth water surface and a rough surface, which was newly introduced in this paper. Although the use of the boundary r_S does not affect the final mathematical form obtained in the previous paper, the physical meaning of the

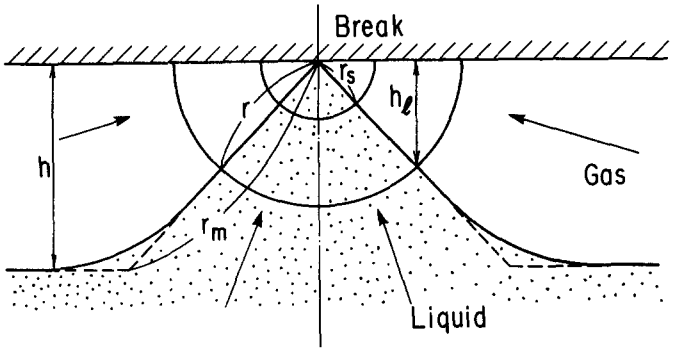

Figure 2. Coordination system of the present model for the top break.

present model has been clarified. The assumptions for the present model are applied only in the smooth surface region $r > r_S$ and are summarized as follows:

(a) The velocity and water surface profile are symmetrical around a break located on an infinite flat plane.
(b) Liquid and gas flow separately.
(c) The two-phase interface is smooth and stable.
(d) The thickness of the velocity boundary layer is small.
(e) Fluid velocity is a function of only the distance from the break.
(f) The energy dissipation produced by the relative motion of the two phases should be minimal under a given condition.

The basic idea of the present model is that the relationship between bulk water level, break flow rate and break quality can be determined from analysis of the water surface profile around a break, since only one profile is considered to be possible from the given conditions. The basic equations used in the present model are explained in appendix A, since they were not explained in detail in the previous paper (Yonomoto & Tasaka 1988). As indicated in the previous paper, the water surface can be calculated using Bernoulli's equation and the above assumptions by varying the void fraction ϵ. The calculated results have shown that the conical shape becomes steep with increasing void fraction and, just beyond a certain value of ϵ, the calculated water level is significantly below the bulk water level in a region just outside the boundary r_m. Energy dissipation produced along the two-phase interface in the conical region was found to decrease with increasing void fraction. It is considered that for the water surface profile to have the local level below the bulk water level in some parts is not realistic and, if it exists, energy dissipation is expected to be large due to the unstable geometry. Therefore, from assumption (f), the appropriate void fraction for the present model was considered to be the maximum void fraction with which the local water level was calculated between elevations of the bulk water surface and the break. The void fraction was obtained approximately from the hydraulic condition at r_m. This is because with the increasing void fraction, the calculated water level is below the bulk water level just outside r_m, as mentioned above. The final form showing the relationship between the water level, flow rate and void fraction obtained from the present model is as follows:

$$\epsilon = -A(1-B) + \sqrt{A^2(1-B)^2 + 2A}, \qquad [1]$$

$$A = \frac{2\pi\sqrt{2g\rho_G\,\Delta\rho}\,h^{2.5}}{3^{1.5}W_{SG}B} \qquad [2]$$

and

$$B = \frac{W_{SG}}{W_{SL}}\sqrt{\frac{\rho_L}{\rho_G}}, \qquad [3]$$

where W_S is the single-phase break flow rate defined with the differential pressure between the bulk and the boundary r_S, g is the acceleration due to gravity, h is the bulk water level relative to the

break, ρ is the density, $\Delta\rho$ is the density difference between the liquid and gas and the subscripts G and L mean gas and liquid, respectively.

For existing correlations in the literature, the break quality is correlated as a function of h/h_b, where the onset water level for the entrainment h_b is determined from an analogy of Lubin & Springer's (1967) theoretical result, which has the following form for the top break:

$$\frac{W_{SG}}{A_B\sqrt{gd\rho_G\,\Delta\rho}} = C1\left(\frac{h_b}{d}\right)^{C2}, \qquad [4]$$

where d is the break diameter and A_B is the break flow area. Lubin & Springer's (1967) theoretical results showed C1 and C2 to be 3.22 and 2.5, respectively. When C2 = 2.5, the break diameter d vanishes from [4], indicating the break can be considered as a punctual sink. Therefore, from assumption (a), the value of 2.5 was used for C2 for consistency with the assumption in the present model. From [1] and [4], and a relation that ϵ should be 1.0 when $h/h_b = 1.0$, ϵ was expressed as follows:

$$\epsilon = -C + \left[C^2 + \frac{1}{B}\left(\frac{h}{h_b}\right)^{2.5}\right]^{0.5}, \qquad [5]$$

where

$$C = 0.5\frac{1-B}{B}\left(\frac{h}{h_b}\right)^{2.5}. \qquad [6]$$

The result that the break void fraction and thus the break quality, i.e. $\epsilon W_{SG}/(\epsilon W_{SG} + (1-\epsilon)W_{SL})$, are expressed as functions of h/h_b, agrees with previous studies in the literature.

Since details of this analysis are available in the previous paper (Yonomoto & Tasaka 1988), only additional discussions concerning the use of the boundary r_S and justification of the present model are described hereafter.

First, the newly introduced idea of the boundary of r_S is discussed. This idea was introduced to better explain the characteristic of the present model that the assumptions do not have to be satisfied in the close vicinity of the break. Depending on the conditions expected for the LOCA problem, the fluid velocity may be accelerated up to the order of 100 m/s when approaching the break, since the gas velocity is roughly proportional to $1/r^2$. Under this condition the surface may not be considered stable, due to hydraulic instability. Surface waves and entrainment of small liquid droplets may occur due to the relative velocity. The assumption of a smooth and stable surface is inappropriate for this flow condition. However, it should be noted that the void fraction expressed by [1] is determined by the hydraulic condition at r_m. The behavior in the region $r < r_S$ does not affect that at r_m directly, but it affects the location of r_S and thus, W_S in [1]. Therefore, as long as $r_m > r_S$ and the flow behavior in the region $r < r_S$ does not affect that in the region $r > r_S$, the present model can be used.

Secondly, the use of Bernoulli's equation is discussed. In the present analysis, the fluid velocity v_G or v_L is assumed to be the same as the average fluid velocity, i.e. the volumetric flow rate divided by the flow area. This assumption concerning the fluid velocity is justified when the boundary layer thickness is sufficiently small. Although exact estimation of the boundary layer thickness has not been performed, it is thought to be useful to see the flow behavior of the two-dimensional flow toward a mass sink. The boundary layer thickness on the smooth wall has been analyzed for two-dimensional flow toward the mass sink located on the z-axis of the cylindrical (r–θ–z) coordinates system, where the flow field is surrounded by two walls expressed by, for example, $\theta = \theta_1$ and $\theta = \theta_2$, and intersects at the z-axis (Landau & Lifshitz 1970). The analysis results showed that the boundary layer thickness was so small that the whole flow field could be treated as a potential flow. Although the present flow model is three-dimensional, the result that the boundary layer thickness on the smooth surface is small for accelerated flow toward a mass sink may be applied to the present situation, at least as a first approximation. It should be noted that when the void fraction is close to 0.0 or 1.0, i.e. the flow area in one phase becomes small, the boundary layer thickness cannot be neglected. In this case, assumption (d) is not satisfied, thus the present model is not appropriate.

The assumption of a smooth surface should also be checked when using Bernoulli's equation. The fluid velocity may be accelerated beyond a stability limitation, such as the critical velocity for slug flow. However, the limit of the smooth surface region for the present model is not determined solely by the critical velocity for slug flow, since the fluid is accelerated into the break in a very short time period. Therefore if the rate of increase of the wave amplitude is small, and thus the height of the wave is not too large compared with the flow area, the region can be considered as a smooth surface region for the present model, even when the velocity exceeds the stability limit for steady-state flow.

Finally, the applicability of assumption (f) is discussed. This assumption was introduced as an analogy of the principle of minimum entropy production rate. It is known that a steady-state thermodynamic process is characterized by a minimum in the rate of entropy production, subject to the limitation that the process is close enough to equilibrium that linear phenomenological laws govern the rate of entropy production (Glansdorff & Prigogine 1977). When the velocity is small, the steady-state velocity distribution for single-phase flow is determined so that the energy dissipation is minimal (Glansdorff & Prigogine 1977). The limitation of the near-to-equilibrium condition indicates that when the condition is far from equilibrium and/or the hydraulic instability plays a dominant role, this principle cannot be used rigorously. It has not been investigated rigorously whether the present problem requires minimum energy dissipation or not. In expectation that the fluid particles in the present situation would avoid flow resistance, if possible, and therefore this idea would give at least an approximation to the rigorous solution, this minimum entropy production rate idea was introduced in the present model as an assumption rather than as the principle.

This principle was used for the analysis of vertical annular two-phase flow (Zivi 1964), in which the minimum entropy production is assumed to be equal to the minimum kinetic energy without considering the potential energy. The potential energy cannot be neglected for the present model using Bernoulli's equation. Therefore, the model used by Zivi cannot be used directly.

More recently, this principle was discussed by Joseph *et al.* (1984) when they studied the flow of two immiscible liquids, with different viscosities, in a pipe. This problem has a continuum of solutions corresponding to arbitrarily prescribed interface shapes. They conducted a linear stability analysis to determine which of these solutions were stable. Their conclusions have shown that although there is some truth in the dissipation principle, it is not always true when considering the flow instability.

The present problem is similar to that of Joseph *et al.* (1984) in the sense that both include the task of determining the interfacial geometry, i.e. one interfacial geometry should be determined from many geometries for given flow rates and pressure fields. Their conclusions may be applied to the present study as follows. When the minimum energy dissipation law is used with the steady-state balance analysis, as in the present study, the flow instability cannot be considered correctly. Therefore, it may happen that the solution obtained in such an analysis is unstable, and thus is not observable. The stability of the flow cannot be investigated correctly with the present steady-state calculation. The stability should be checked carefully by comparison with observational results, since if the flow field is significantly unstable, not only assumption (f) but also assumptions (b)–(d) cannot be used.

Although the dynamic analysis has not been performed, the stability of the flow was estimated from the shape of the two-phase interface for the present study. As mentioned before, the local water level was calculated to be significantly below the bulk water level just outside r_m when the void fraction became slightly larger than a certain value. Such a flow configuration is intuitively expected to be unstable. Therefore, the energy dissipation of such a flow configuration is supposed to increase. On the other hand, the energy dissipation due to the interfacial drag decreases with increasing void fraction for the top break. Therefore, the energy dissipation is supposed to be at a minimum around the maximum void fraction with which the local water level is calculated between the bulk water surface elevation and the break elevation.

From the above discussions, it is concluded that the flow behavior around the break is very important when considering the applicability of the present model to the actual problem. In particular, a comparison of the size of r_S and r_m is needed. In order to use the present model, r_m should be larger than r_S, and the surface around r_m should be smooth and stable and unaffected

by the region $r < r_S$. This point will be checked by comparison with observational results in section 4.

2.2. *Improvements of the proposed model*

As mentioned previously, the single-phase flow rates W_{SG} and W_{SL} should be calculated using the differential pressure between the bulk region and the boundary r_S in order to use [1]. Generally this is difficult, especially when the pressure loss is large in the region $r < r_S$ and/or the break geometry is a nozzle with a large length/diameter ratio. This is because complicated phenomena such as choking, phase change, momentum and mass exchange between the two phases can occur in this case, which make the prediction of the pressure at r_S from the given upstream and downstream bulk conditions difficult. Usually, the given conditions are the upstream and downsteam bulk pressures for the LOCA problem. The model without W_{SG} and W_{SL} is, therefore, appropriate for the LOCA analysis. Based on the analytical procedure explained in the previous paper (Yanomoto & Tasaka 1988), and using the break quality x and the break flow rate W instead of ϵ, W_{SG} and W_{SL}, the following equation was obtained, which shows relation between x, W and h:

$$W = 2^{2.5}\pi\sqrt{g\rho_G\Delta\rho}\frac{h^{2.5}}{3^{1.5}}\frac{1}{x}\left(\frac{1-x}{x}\sqrt{\frac{\rho_G}{\rho_L}}+1\right). \quad [7]$$

In order to use the present entrainment correlation [7] for the LOCA analysis, the break flow model must be combined. Generally, the break flow model, or the critical flow model, shows a relationship between the break quality, the break flow rate and so on. Therefore, by combining the present model and the break flow model, the break flow rate and the break quality can be calculated from given upstream and downstrem pressures and the water level in the upstream region.

A similar procedure was used for side and bottom breaks and the resulting expressions are summarized in appendix B.

3. EXPERIMENTS

Air–water experiments were conducted to investigate the entrainment behavior and to assess the present model. A 190 × 190 mm square duct was used as a horizontal main line, instead of a round pipe, to simplify the phenomena. The length of the main line was 7.75 m. A break simulation line was connected to the main line at 5.5 m from the inlet. The entrainment for upward, sideward or downward break orientations was investigated. Several break geometries were tested: a sharp-edged orifice with a diameter of 10, 15 or 20 mm; or a tube of length 150 mm and dia 10 mm. The experiments were conducted under the steady-state condition at room temperature. The pressure range tested was between 0.4 and 0.7 MPa. The experimantal data were recorded manually, which required that the steady-state condition leasted at least 2 min. More detailed information is available in Yonomoto & Tasaka (1988).

4. EXPERIMENTAL RESULTS

4.1. *Entrainment behavior*

The experimental results showed that the primary parameters concerning the entrainment behavior were the differential pressure across the break and the water level in the main line. Stable entrainment occurred with increasing differential pressure across the break and/or with closer proximity of the bulk water surface to the break elevation. Unstable and intermittent entrainment was observed between the continuous and no entrainment conditions, as indicated in all the previous results in the literature.

For the top break, the formation of vortices and waves also affected the entrainment behavior significantly, as observed by Smoglie (1984; Smoglie & Reimann 1986) and Schrock *et al.* (1986). The characteristics of the entrainment behavior for the top break can be highlighted by plotting the normalized water level data against the normalized gas velocity data in the main line, as shown in figure 3. The water level relative to the break is normalized by the onset water level for the entrainment, which is calculated with [4] with C1 = 4.35. The gas velocity on the upstream side in

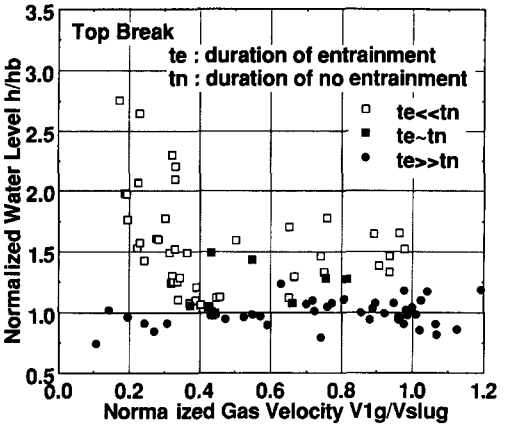

Figure 3. Entrainment characteristic for the top break.

the main line is normalized with the critical velocity for slugging. The Mishima & Ishii (1980) correlation was used as the slugging criterion:

$$v_{slug} = 0.487 \sqrt{\frac{\Delta\rho g h}{\rho_G}} + v_{L1}. \quad [8]$$

In figure 3, the experimental data were visually classified into three groups according to duration of entrainment compared with the period of no entrainment. The data represented by $t_e \ll t_n$ indicate that entrainment occurred intermittently. This group includes the data indicating the onset condition for entrainment. The data represented by $t_e \gg t_n$ indicate the continuous entrainment condition. The data represented by $t_e \sim t_n$ correspond to the data which was difficult to classify as one of the two extreme cases above.

Entrainment first occurred due to vortex formation in the main line. Most of the data represented by $t_e \ll t_n$ and $t_e \sim t_n$ were affected by the vortex flow. The direction of the vortex and the movement of the vortex axis were very unstable. Typical behavior of this unstable entrainment was as shown in pictures taken by Smoglie & Reimann (1986). Figure 3 shows that intermittent entrainment occurs at a relatively high value of h/h_b when the normalized gas velocity is small and at a relatively low value of h/h_b when the gas velocity is large. This is probably due to the suppression of the vortex formation by the gas flow in the main line. The vortex flow was also suppressed by decreasing the value of h/h_b. Significant vortex flow was not observed when continuous and stable entrainment occurred.

With increasing gas velocity in the main line, the flow regime in the main line changed from smooth stratified flow to wavy flow. The amplitude of the wave was about 1 mm at a normalized gas velocity of 0.5 and about 5 mm at a normalized gas velocity of 1.0. Liquid entrainment was enhanced by the wave flow. More liquid was entrained when the peak of the wave approached the break.

The flow behavior for continuous entrainment under the symmetrical upstream condition is described in detail hereafter since it is important to discuss the applicability of the present model. For this flow condition, slug flow did not occur and the shape of the water surface around the break was symmetrical, as shown in figure 4.

Typical pressure, bulk water level and break diameter were 0.7 MPa, 2 and 1 cm for the top break. A typical gas velocity in the bulk region was 1 m/s, corresponding to a normalized velocity of 0.5 (defined with [8]). The observed wave amplitude was about 1 mm in the bulk region. The boundary of the region of water level change r_m was about 30 mm from the break. The gas velocity increased to about 6 m/s at r_m, corresponding to a normalized velocity of 3. This means that the velocity was beyond the stability criterion for steady flow. However, the wave height was about 2 mm in the region around r_m. Although the gas velocity was estimated to be accelerated to about 200 m/s at $r = 5$ mm, the wave amplitude did not develop in this region 5 mm $< r <$ 30 mm. The frequency of the wave was about 10 Hz in this region. In the region $r < 5$ mm, the wave disappeared but entrainment of many small liquid droplets with a diameter of the order of 0.1 mm was observed.

Therefore, the region $r < 5$ mm looked white. The boundary around 5 mm may be considered to be r_S, defined in section 2.1. The diameter of the two-phase region at the break inlet was about 4 mm.

From the above observations, the assumption of separate flow is considered to be applied in the region $r > r_S$. The flow behavior at r_m was not completely smooth, but the amplitude of the wave was much smaller than the water level of 20 mm. The entrainment of small droplets did not occur at r_m. Therefore, the observed flow behavior is considered to be similar to that expected in the present model.

For the side break, the onset conditions for entrainment were not significantly affected by the upstream flow conditions because vortex and wavy flow did not occur significantly in the present test condition. Vortex flow occurred only when the amount of entrainment was very small for gas entrainment. The vortex flow is thought to be suppressed by the wall. For liquid entrainment, which occurred when the water surface was lower than the break elevation, liquid was entrained along the wall. However, for gas entrainment, the entrained air showed a tendency to flow off the wall, especially when the gas flow rate was relatively small. This observational result does not agree with the assumption of the symmetrical shape of the water surface around the break in the present model. The present model assumes that the axis of the symmetry should be on the wall for the side break.

Figures 5 and 6 show the entrainment behavior for liquid and gas entrainment, respectively, under the condition of symmetrical flow around the break. The figures show that the shape of the air–water interface was approximately semiconical except in the close vicinity of the break. When crossflow was present, the air–water interface was distorted due to the liquid crossflow, as shown in figures 7 and 8.

As well as being observed for the top break, the entrainment of many small liquid droplets was observed in the region $r < \sim 5$ mm. The color of this region was white due to the entrained small droplets, for both the gas and liquid entrainment conditions, indicating the water surface is not smooth in this region. However, since wave flow did not occur in the bulk region, the flow behavior around r_m was smooth and calm for the symmetrical upflow condition. A typical value of r_m was about 20 mm, which satisfies the condition of $r_m > r_S$. Of course, when h is small, the condition $r_m > r_S$ is not satisfied, since r_m also becomes small. The assumption of the punctual sink cannot be used when h is small. Therefore, the present model cannot be used when h is too small.

The observational results for the side break continuous entrainment behavior under the symmetrical upstream condition indicate that the flow behavior is similar to that expected in the present model, except when h is too small and the entrained gas tends to flow off the wall.

Entrainment was significantly affected by the upstream liquid flow condition in the main line for the bottom break. The occurrence of vortex flow and liquid crossflow significantly affected entrainment, as observed by Smoglie & Reimann (1986). The typical behavior of stable vortex-free entrainment under the symmetrical flow and crossflow conditions, and stable vortex-induced entrainment are shown in figures 9–11.

(Figs 4–6 Opposite)

Figure 4. Top break under symmetrical flow conditions ($d = 10$ mm, main line pressure $P = 0.69$ MPa, differential pressure across the break $\Delta P = 0.30$ MPa, $h = 18$ mm, break mass flux $G = 2350$ kg/m^2 s, $x = 0.29$).

Figure 5. Side break liquid entrainment under symmetrical flow conditions ($d = 15$ mm, $P = 0.67$ MPa, $\Delta P = 0.54$ MPa, $h = 23$ mm, $G = 3460$ kg/m^2 s, $x = 0.33$).

Figure 6. Side break gas entrainment under symmetrical flow conditions ($d = 15$ mm, $P = 0.69$ MPa, $\Delta P = 0.17$ MPa, $h = 31$ mm, $G = 10300$ kg/m^2 s, $x = 0.0076$).

(Figs 7–9 on p. 754)

Figure 7. Side break liquid entrainment under liquid crossflow conditions ($d = 15$ mm, $P = 0.66$ MPa, $\Delta P = 0.54$ MPa, $h = 28$ mm, $G = 2220$ kg/m^2 s, $x = 0.558$, $v_{1L} = 0.23$ m/s, $v_{2L} = 0.22$ m/s).

Figure 8. Side break gas entrainment under liquid crossflow conditions ($d = 15$ mm, $P = 0.69$ MPa, $\Delta P = 0.13$ MPa, $h = 38$ mm, $G = 8970$ kg/m^2 s, $x = 0.00245$, $v_{1L} = 0.34$ m/s, $v_{2L} = 0.29$ m/s).

Figure 9. Bottom break gas entrainment under symmetrical liquid flow conditions ($d = 15$ mm, $P = 0.69$ MPa, $\Delta P = 0.57$ MPa, $h = 29$ mm, $G = 12100$ kg/m^2 s, $x = 0.0315$).

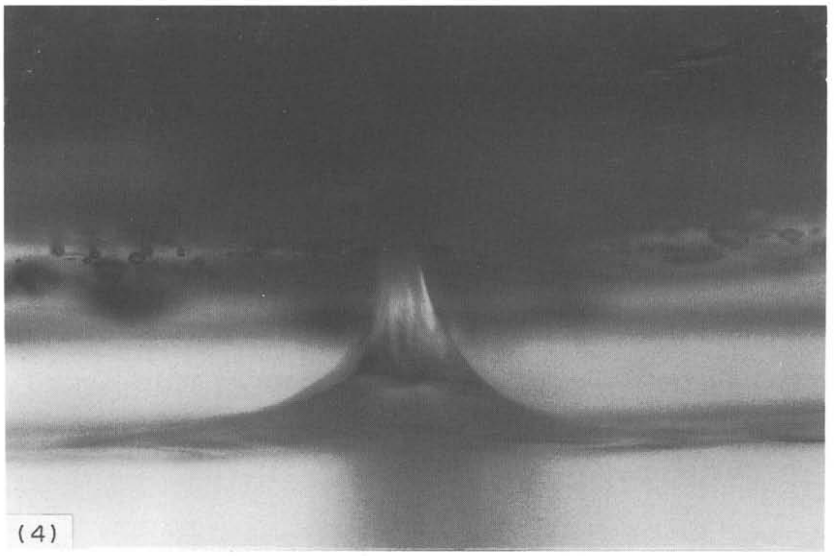

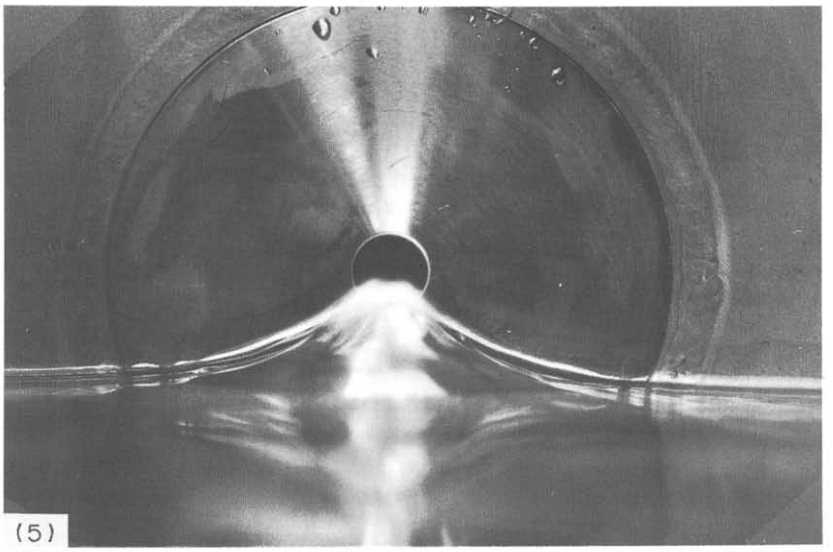

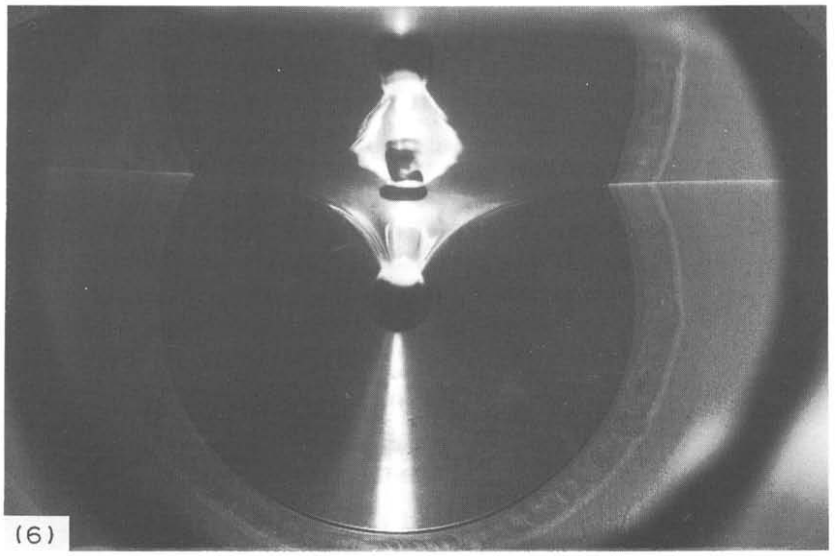

Figs 4–6: *legends opposite.*

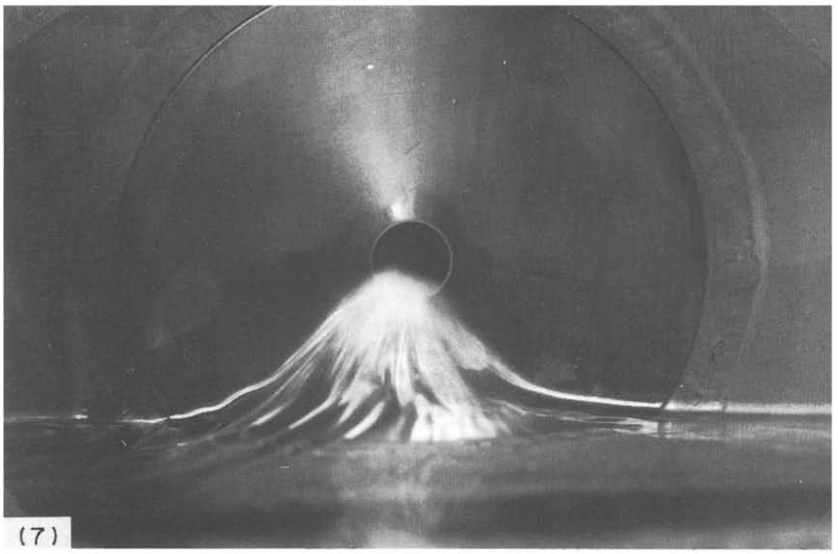

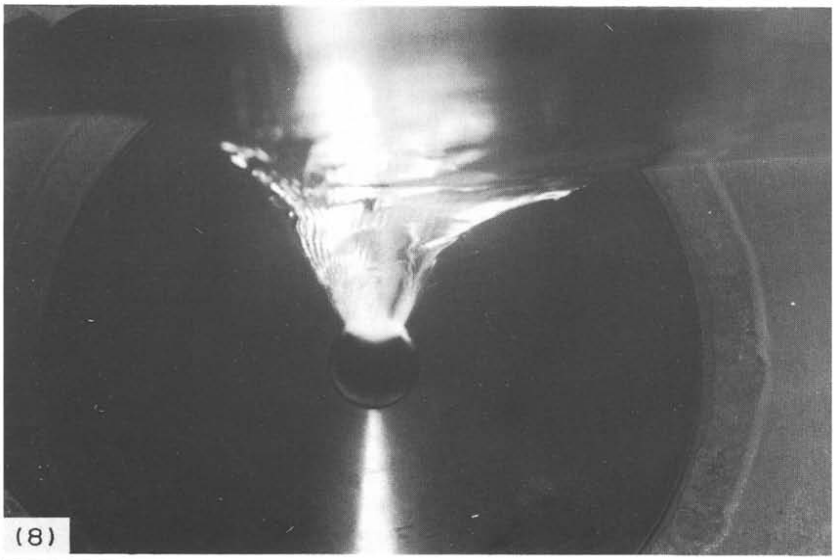

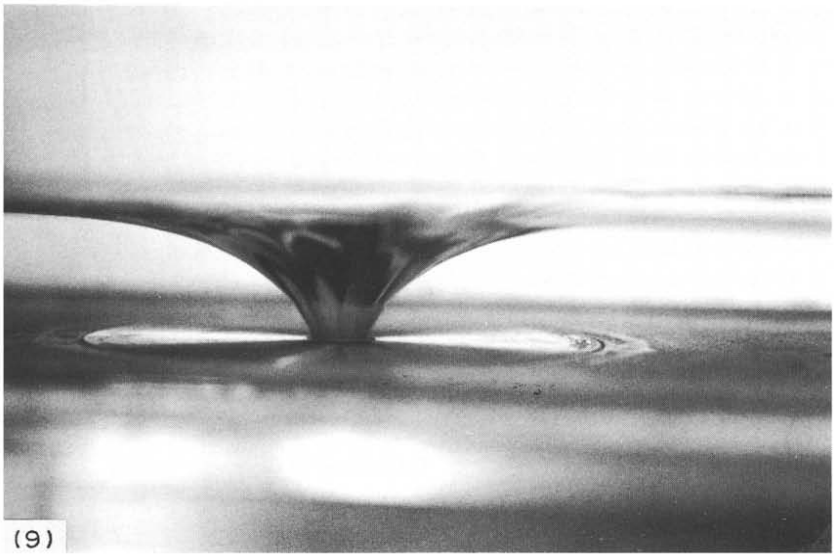

Figs 7–9: *legends on p. 752.*

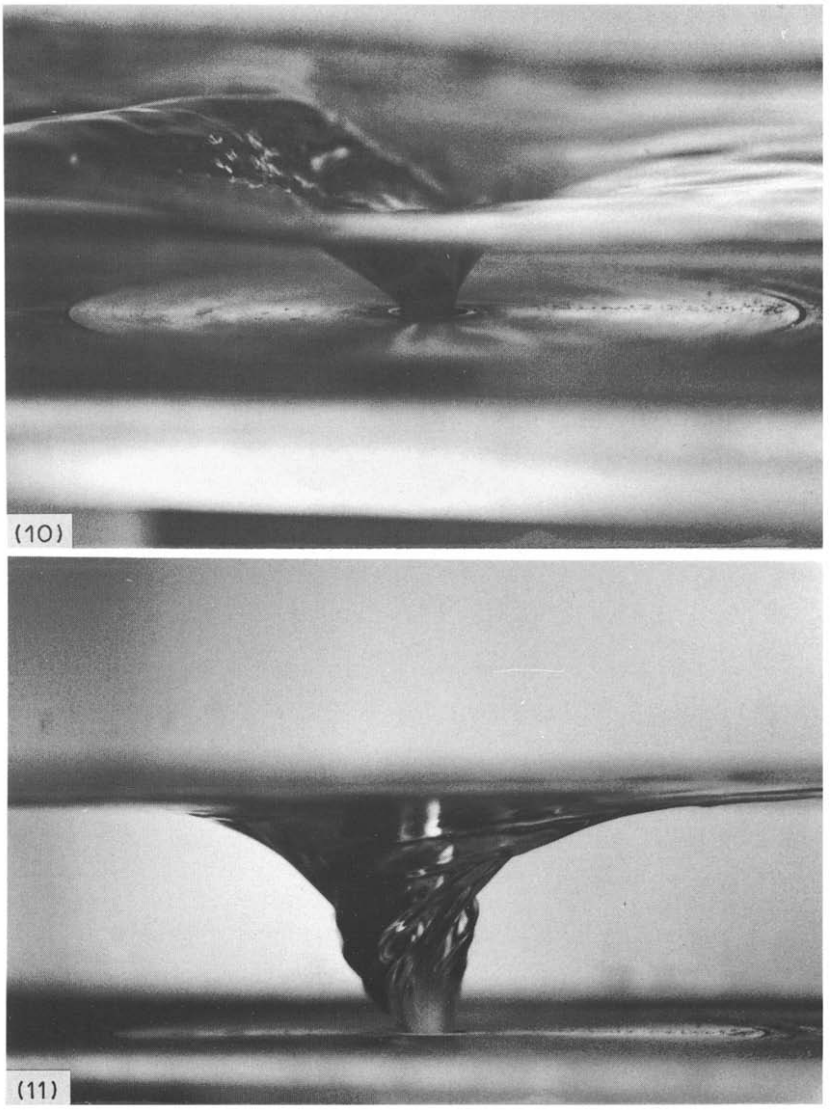

Figure 10. Bottom break gas entrainment under liquid crossflow conditions ($d = 10$ mm, $P = 0.69$ MPa, $\Delta P = 0.59$ MPa, $h = 24$ mm, $G = 7780$ kg/m^2 s, $x = 0.0276$, $v_{1L} = 0.33$ m/s, $v_{2L} = 0.13$ m/s).

Figure 11. Bottom break gas entrainment under vortex flow conditions ($d = 10$ mm, $P = 0.69$ MPa, $\Delta P = 0.341$, $h = 33$ mm, $G = 10000$ kg/m^2 s, $x = 0.0104$).

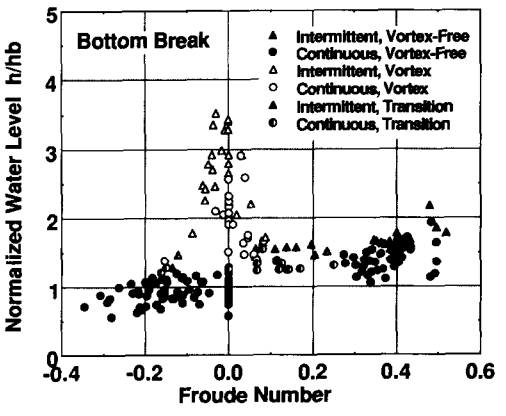

Figure 12. Entrainment characteristic for the bottom break.

Table 1. Values for C1 expressing onset conditions for entrainment

	Present study		Smoglie *et al.*		
	First	Continuous	First	Continuous	Anderson
Bottom (vortex flow)	0.3 ± 0.2	0.7 ± 0.1	0.23	—	—
Bottom (crossflow)	1.3 ± 0.3	1.6 ± 0.3	0.94	1.1	1.27
Side (gas entrainment)	1.5 ± 0.5	3.0 ± 0.2	2.61		2.09
Side (liquid entrainment)	4.0 ± 1.0	4.0 ± 1.0	3.22	4.21	
Top (smooth surface)	0.7 ± 0.3	5.0 ± 1.0	0.35	—	—
Top (wavy)	1.7 ± 0.5	3.6 ± 0.2	—		—

The conditions for the occurrence of vortex flow could be correlated with the Froude number $v_2\sqrt{gh_2}$ and the normalized water level h/h_b, where the subscript 2 indicates the outlet side in the mainline, and a negative value of v_2 means the flow direction is toward the break. The results are shown in figure 12. The figure shows that vortex flow occurs when the following conditions are satisfied:

$$\left|\frac{v_2}{\sqrt{gh_2}}\right| < 0.25,$$

and

$$\frac{h}{h_b} > 1.2, \qquad [9]$$

where h_b is calculated using C1 = 4.35. When vortex flow does not occur, the liquid crossflow rate in the main line significantly affected entrainment. The shape of the water surface was distorted by the crossflow, as shown in figure 10. When the fluid was supplied symmetrically to the break, the conical shape of the water surface was observed for stable entrainment, as shown in figure 9. The shape of the water surface for the symmetrical flow condition was similar to that for the top break, except that the wave did not occur at r_m. The color of the surface was white in the region $r \lesssim 5$ mm, indicating that the surface is not smooth in this region as observed for the other break geometry conditions. The boundary $r_S \sim 5$ mm was smaller than the boundary of r_m having typical value of 20 mm. The flow around $r = r_m$ was stable and smooth, as assumed in the present model.

4.2. Onset condition for entrainment

The onset conditions for entrainment have been correlated with [4] by changing C1 to agree with the experimental data in the previous works in the literature. Equation [4] is rewritten as

$$C1 = \frac{4\,W_k}{\pi\sqrt{g\rho_k\,\Delta\rho}\,h_b^{C2}}, \qquad [10]$$

where the subscript k means gas for the liquid entrainment and liquid for the gas entrainment. Most of the previous experimental results have indicated that the value for C2 in [10] is 2.5.

The present experimental data concerning the onset of entrainment were correlated with [10] and the results are shown in table 1. A smaller value of C1 means entrainment occurs at a larger relative water level. Thus, the value for intermittent entrainment is smaller than that for continuous entrainment, as mentioned in the previous section. Although many parameters affect entrainment, the effects have been simplified in table 1. The values corresponding to vortex flow and crossflow for a bottom break, and wavy and smooth stratified flow are listed in the table. For a side break, the effects of such parameters were not as significant, as mentioned in the previous section. The value of C1 has relatively large uncertainty, as shown in table 1. One reason for this arises from

Table 2. Experimental conditions of data bases in the literature

	KfK	INEL	UCB	CEA
Max. press (MPa)	0.5	6.2	1.0	2.0
Fluid	A–W[a]	S–W[a]	A–W, S–W	S–W
Horizontal pipe dia (mm)	206	284	102	135
Break dia (mm)	6, 8, 12, 20	34	3, 4, 6, 10	20

*A–W, air–water; S–W, steam–water.

the difficulty in visual determination. The other reason is that the entrainment behavior is very unstable when it begins. This is shown in figures 3 and 12 for top and bottom breaks, respectively. The data indicated by $t_e \ll t_n$ in figure 3 and the intermittent entrainment in figure 12 include the onset data, which shows relatively large scattering.

Table 1 also shows the results by Smoglie & Reimann (1986; Smoglie 1984) and Anderson & Owca (1985); the test conditions for them are listed in table 2 and will be mentioned in the following section. The onset condition was visually determined for the data by Smoglie & Reimann and was determined by a change in the differential pressure across the break for the data and Anderson & Owca. Considering the scattering nature of the onset data, it can be said that the results are almost the same for the three experiments listed in table 1.

The theoretical value for the onset of entrainment obtained by the present model is 4.35 for top and bottom breaks and 6.16 for the side break. These values are different from the data shown in table 1. The reason for this disagreement concerning C1 is thought to be that the present model is based on stable, vortex-free, no crossflow and no wavy flow conditions, while they affect significantly the onset condition. This means the present model cannot be used when the amount of entrainment is relatively small.

5. COMPARISON BETWEEN THE THEORY AND THE EXPERIMENTAL DATA

5.1. Assessment of the present model

As discussed in section 4, the observed flow behavior around r_m was smooth and stable, as assumed in the present model, when experimental conditions were similar to the present assumptions. Therefore, the use of the present model for the analysis of the present experiment result is justified. The data selected from the present data base for the assessment were those obtained under conditions of: (i) symmetric flow upstream of the break; (ii) large distance between the break entry and bulk water elevations; and (iii) continuous entrainment.

The first condition, the symmetrical flow, means symmetrical liquid flow in the main line around the break for the side and bottom breaks, and symmetrical gas flow for the top break; because the gas crossflow for the side or bottom breaks and the liquid crossflow for the top break did not significantly affect the entrainment behavior for the present test conditions. The second condition means that the relative water level is larger than a break diameter for the top and bottom breaks, and a break radius for the side break. The third condition means that data taken under the intermittent entrainment condition is excluded for the assessment of the present model.

The first comparison results of the predicted and measured break mass fluxes are shown in figure 13, where the predictability, expressed as the predicted value divided by the experimental data, is plotted against the normalized water level, break mass flux and break quality. The break flow rates were predicted using the measured data of pressure, temperature, break quality and bulk water level, and [7] for the top break, and the corresponding equation in the appendix for the other break conditions.

The break flow rate was overpredicted by about 50% for the side gas entrainment condition, as shown in figure 13, which is the most significant disagreement among the tested break geometries. This disagreement is probably because entrained gas tends to flow off the wall, although the central axis of the entrained gas is assumed to be on the wall in the model (as discussed in section 4).

Figure 13 shows that the break mass fluxes are underpredicted when the normalized level is <0.6 for the side break liquid entrainment, and overpredicted when the level is >1.0 for the bottom and side breaks. This disagreement corresponds to the overprediction for the bottom break for quality <0.02, and the dependency that the break flow rate becomes overpredicted with increasing break quality for the side liquid entrainment appeared in the predictability vs quality plane.

The reason for the disagreement regarding the relatively high water level may be because the present model is not appropriate when the void fraction is near 1 or 0, as discussed in section 2.1. The result that stable entrainment is observed, even when the normalized water level exceeds 1, also indicates that the present model is not appropriate when the entrainment rate is not large.

The reason for the underprediction of the side liquid entrainment may be due to the effects of the break size, i.e. typical values of water level and break diameter are 2 and 1 cm, respectively

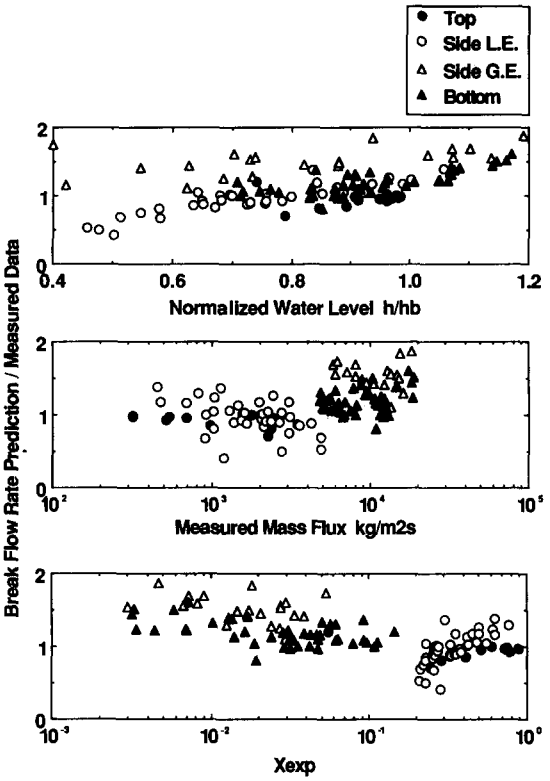

Figure 13. Comparison of predictions and the present experimental data for break mass flux under symmetrical flow conditions.

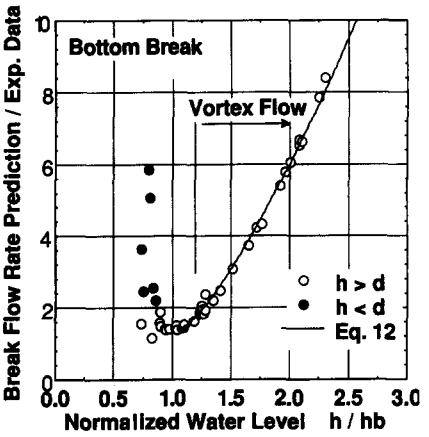

Figure 14. Effects of water level on the predictive capability of the break flow rate under bottom break conditions, with a Froude number between 0.0 and 0.25.

for the side liquid entrainment, indicating that the break size is not negligibly small. The effects of the break size are considered more significant for the side break than for the top and bottom breaks, because the elevation difference between the bulk water surface and the nearest portion of the break hole is significantly affected by the break size for the side break.

Although the above-mentioned disagreements can be observed in figure 13, most of the data were well predicted with an accuracy of about 30% for the side liquid entrainment, top break and bottom break. The data compared in the figure include those taken with sharp-edged orifices and the tube with a length/diameter ratio of 15. No effects related to the different break geometries were found, as expected. The above-mentioned agreement indicates that the effects of water level, differential pressure and density are well accounted for in the present model. Therefore, the present model may be considered as a base for the analysis of entrainment.

5.2. Empirical modification

The other important parameters observed in the experiment but not taken into consideration in the model are vortex flow, crossflow, wavy flow etc. These effects were investigated experimentally. The empirical equations were formulated on the basis of the present model.

For the empirical modification, the normalized water level h_b is often used via [10]. Although the onset water level for entrainment is significantly affected by the flow conditions, as described in the previous section, the value of h_b is simply calculated using the present theoretical results of C1, i.e. 4.35 for the top and bottom breaks and 6.16 for the side break. Therefore, the calculated value of h_b does not represent the onset water level for entrainment, as discussed in the section 4.2. The onset water level for continuous entrainment can be calculated by using the empirically modified entrainment correlation, described hereafter, with $x = 1.0$ and 0.0 for liquid and gas entrainment, respectively.

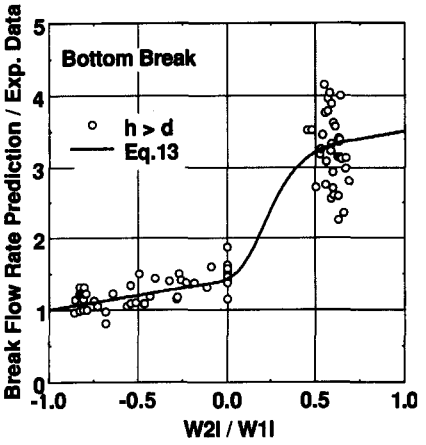

Figure 15. Effects of the water flow rate ratio on the predictive capability of the break flow rate under bottom break conditions, with a Froude number of >0.25.

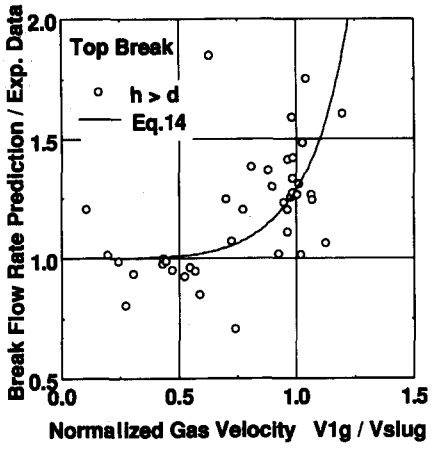

Figure 16. Effects of gas velocity in the main line on the predictive capability of the break flow rate for the top break.

The present correlation expressing the relationship between break mass flow rate, water level and pressure was empirically modified by using a modification factor C as follows:

$$W_{cal} = \frac{1}{C} W_{th}, \qquad [11]$$

where W_{th} is the break flow rate calculated with the present theoretical entrainment correlation.

For the bottom break, vortex flow and crossflow significantly affected entrainment, as mentioned in the previous section. Figure 14 shows the effects of the water level on the predictability for the break flow rate. The data used in the figure are selected from data with a Froude number $v_2/\sqrt{gh_2}$ between 0 and 0.25. Vortex flow was observed when $h/h_b > 1.2$. The figure shows the break flow rates are overpredicted when vortex flow occurs, and also overpredicted when the water level becomes small compared with the break size. These disagreements indicate the importance of the effects of the break size and vortex flow.

When vortex flow did not occur, crossflow in the main line affected the entrainment significantly. Figure 15 shows the effects of a ratio of the liquid inlet and outlet flow rates in the main line on the predictability under the vortex-free condition, where W_{2L} and W_{1L} represent liquid flow rates in the main line on the outlet and inlet sides, respectively. The figure shows that the break flow rate is significantly overpredicted with increasing values of W_{2L}/W_{1L}.

The effects of vortex flow and crossflow were correlated by using the results shown in figures 14 and 15 for the bottom break, which are expressed as follows:

for the vortex flow condition,

$$C = 5.1\left(\frac{h}{h_b} - 1.08\right)^{1.3} + 1.4; \qquad [12]$$

and

for the vortex-free flow condition,

$$C = 1.7 \exp\left[-1.0\left(\frac{W_{2L}}{W_{1L}} - 1.2\right)^8\right] + 0.4\frac{W_{2L}}{W_{1L}} + 1.4. \qquad [13]$$

Whether vortex flow occurs or not is estimated from the relationship expressed by [9]. The values calculated with [12] and [13] are shown in figures 14 and 15, respectively.

For the top break, the effects of wavy flow were considered. Figure 16 shows the effects of the gas velocity in the main line on the predictability of the present model, where the gas velocity is normalized with v_{slug}. The figure shows that the present model predicts the break flow rate well when the normalized gas velocity is relatively low, i.e. the upstream flow condition is smooth stratified flow, however, with increasing gas velocity, the present model overpredicts the experimental data—probably due to the effects of wavy flow in the main line.

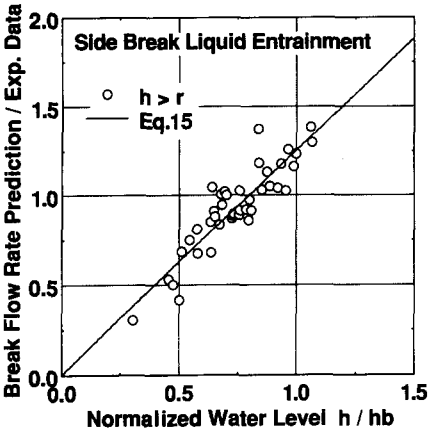

Figure 17. Effects of water level on the predictive capability of the break flow rate for the side break liquid entrainment.

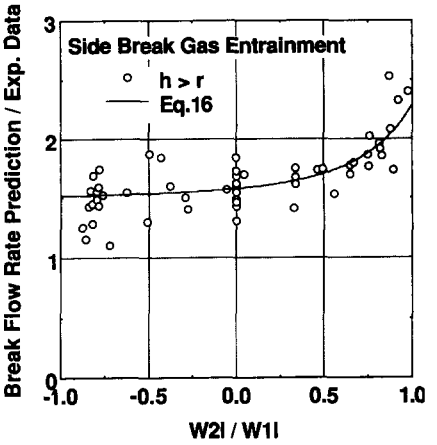

Figure 18. Effects of liquid flow rate ratio in the main line on the predictive capability of the side break gas entrainment.

The experimental data were correlated with the following coefficient, as shown in figure 16:

$$C = \exp\left[0.25\left(\frac{v_{1G}}{v_{slug}}\right)^5\right]. \quad [14]$$

For the side break liquid entrainment, the effects of liquid crossflow were not significant and wavy flow did not occur for the present experimental conditions. However, the dependency of the predictability on the normalized water level was observed, as shown in figure 17. The break mass flow rate was overpredicted with increasing normalized water levels. This tendency was corrected with the following coefficient, as shown in figure 17:

$$C = 1.25\frac{h}{h_b}. \quad [15]$$

For side break gas entrainment, the effects of liquid crossflow were observed. Figure 18 shows overpredictions of the data with a dependency of W_{2L}/W_{1L}. This disagreement was corrected with the following coefficient, as shown in figure 18:

$$C = 1.5 + \frac{\exp\left(0.25\dfrac{W_{2L}}{W_{1L}} - 0.5\right)}{\left(2 - \dfrac{W_{2L}}{W_{1L}}\right)^3}. \quad [16]$$

By using the above empirical modifications, the break flow rates measured under various flow conditions in the main line were correlated with an accuracy of $\pm 30\%$.

6. COMPARISON WITH DATA IN THE LITERATURE

Whether the present empirical correlations can be used beyond the present test conditions will be investigated in this section. In particular, the applicability to the high pressure steam–water condition is of primary concern for the safety analysis of the hydraulic behavior under an accidental condition in the reactor. Four data bases are available in the literature for this purpose, the test conditions of which are listed in table 2. Top, side and bottom break experiments were conducted, except for the INEL group (Anderson & Owca 1985) who conducted only side and bottom break tests. Pressure conditions, the geometry of the test section and the fluids tested differ among the data bases. The difference in the flow conditions in the main line should also be noted because it significantly affects the entrainment behavior, as mentioned in the previous section. Most of the data collected by the INEL and UCB (Schrock *et al.* 1986) groups were obtained under a fixed inlet flow condition to the horizontal pipe. All the data used for this comparison were obtained

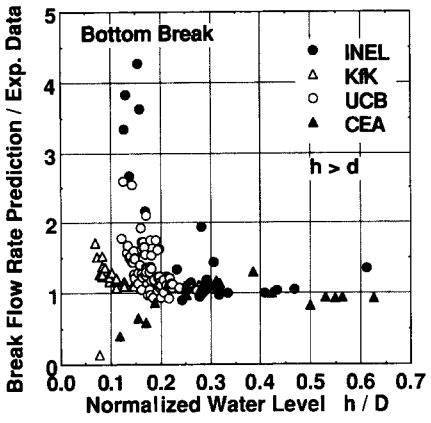

Figure 19. Comparison of the present correlation with data from other data bases for the bottom break.

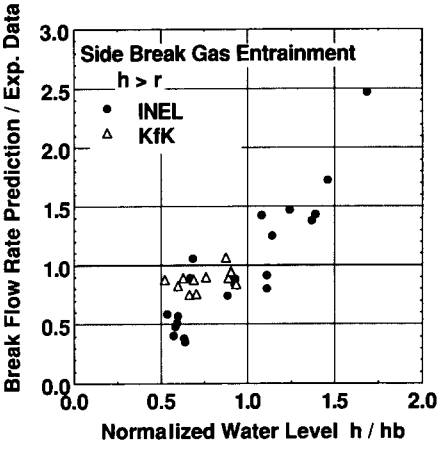

Figure 20. Comparison of the present correlation with data from other data bases, for the side break gas entrainment.

with the no outlet flow condition of the KfK (Reimann & Khan 1983) data base. Most of the data by the CEA group (Masiaszek & Memponteil 1986) used for this comparison were obtained under crossflow conditions which are significantly different from those of the other data bases. For instance, the average liquid velocity on the inlet side of the main line for the bottom break data is about 2.5 m/s for the CEA data base while it is between 0.1–0.4 m/s for the other data bases. It should be noted that no tests were conducted under the symmetrical flow condition in any of the four data bases. Therefore, the present theoretical model cannot be compared directly with their data. Comparison results between the present empirical correlations and the data in the literative will be described hereafter.

Figure 19 shows comparison results for the bottom break. The effects of water level on the predictability of the present correlation are shown in the figure, where the water level is normalized with the diameter of the horizontal main line. The data from the four data bases are compared in the figure. Only the data satisfying the condition of Froude number $|v_2\sqrt{gh_2}|$ of less than 0.25 is plotted from the CEA data base. This is because the water levels are significantly different between the inlet and outlet sides in the main line when the crossflow rate is large for this data base. Such an effect is not taken into account in the present model. The figure shows that the present correlation agrees well with all the data when the normalized water level is larger than 0.2; however it overpredicts when the water level is relatively small. This disagreement indicates that some effects other than those considered in the present model should be taken into account when the water level is relatively low. These include the effects of wall shear, gas vortex, pipe curvature, break size and so on. It should be noted that the present model which is derived from the theoretical model, and the experimental data obtained from low pressure air–water experiments agree well with the high pressure steam–water data obtained by INEL, when the water level is relatively high.

Figure 20 shows comparison results for the side gas entrainment. The effects of water level on the predictability are shown in the figure. The data from the KfK data base are in 20% agreement with the present correlation, indicating that the effect of the pipe wall curvature is not so significant since the experimental conditions are almost the same between the KfK and the present experiments, except for the geometry in the main line. Comparison results for CEA and UCB data bases were excluded from the figure; this is because the data from the CEA and UCB data bases were significantly underpredicted and overpredicted, respectively, and if plotted on the same figure, it becomes too complicated. The reason for this disagreement is not clear. The significant difference in the water level in the main line between the inlet and outlet sides may be responsible for the CEA data. The data from the INEL data base were predicted with about 50% agreement, although the results show the dependency of the predictability on h/h_b. These disagreements show further improvement is necessary for the prediction of the side break gas entrainment.

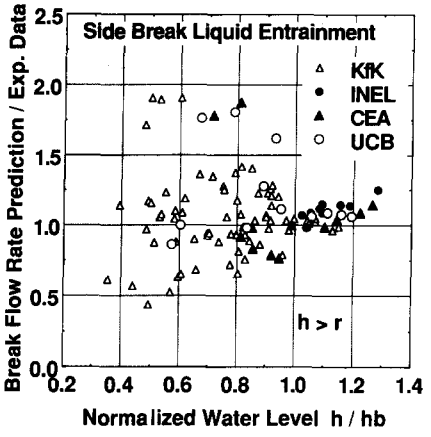

Figure 21. Comparison of the present correlation with data from other data bases for the side break liquid entrainment.

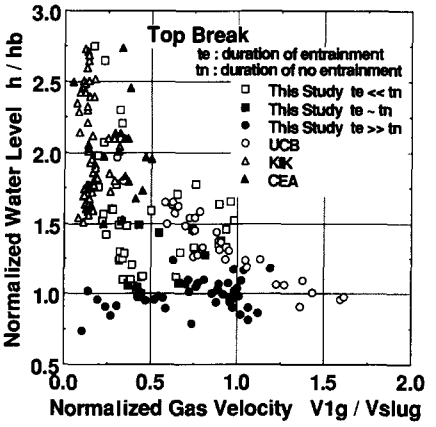

Figure 22. Entrainment characteristic of each data base for the top break.

Figure 21 shows comparison results for the side break liquid entrainment. The figure shows that most of the data are predicted with an accuracy of 30% with the present correlation. Considering the large difference in the test conditions among the data bases, this agreement should be noted. The reason for this agreement may be related to the present experimental result, that the flow conditions in the main line do not significantly affect the side liquid entrainment.

The data from the other data bases in the literature were not predicted accurately for the top break. The reason for this disagreement is considered to be due to the difference in the entrainment behavior between the present experiment and the other data bases. Figure 22 shows comparison of the test conditions of the four data bases for the top break. The normalized water level h/h_b is plotted against the normalized gas velocity v_{1G}/v_{slug} in the main line for each data base. This chart is very important, in order to understand the characteristic of the entrainment for the top break as mentioned in the previous section. The figure shows that most of the data in the literature are in the region of the intermittent entrainment observed in the present test, where the present model cannot be used directly. Therefore it is not appropriate to compare the present correlation with other data bases obtained in the intermittent region. The UCB correlation may be good for a h/h_b condition larger than the present test condition, because it covers a wide range of v_{1G}/v_{slug} compared with the other data bases.

The above comparison results show that the present correlations can be basically applied to stable continuous entrainment behavior under high pressure steam–water conditions for side liquid entrainment and bottom break, with a relatively high water level. Some modification may be required, especially for the bottom break with a relatively low water level and side break gas entrainment.

7. CONCLUSIONS

Improvements for the previously proposed theoretical model, and a detailed experimental study were performed in this paper in order to analyze the entrainment due to a small break in a stratified two-phase region. The previously proposed model was changed into a mathematical form expressing a relation between break flow rate, break quality and bulk water level for the top, side and bottom oriented breaks. The air–water experiment was conducted to investigate in detail the effects of hydraulic parameters on entrainment. The top, side and bottom break experiments were conducted under steady-state conditions. Predictions with the present model agreed very well with the experimental data and did not require the use of any adjustment coefficients when the upstream flow was symmetrical around the break, except during side gas entrainment condition. Effects of the vortex, crossflow, wavy flow and break size were observed in the experiment, and some of them were empirically correlated by modifying the present theoretical correlation. The empirically modified correlations were compared with other data bases in the literature, including high-pressure steam–water conditions. Some modifications were found to be necessary for the bottom break with

a relatively low water level, and for side gas entrainment. However, except for the above disagreements, the agreements were good especially for stable entrainment behavior for the side break liquid entrainment, and bottom break entrainment with a relatively high water level. This indicates that the present model can be basically applied to high pressure steam and water conditions similar to the LOCA conditions in a nuclear reactor.

REFERENCES

ANDERSON, J. L. & OWCA, W. A. 1985 Data report for the TPFL tee/critical flow experiments. EGG-2377, NUREG/CR-4164.

ASAKA, H., KUKITA, Y., YONOMOTO, T., KOIZUMI, T. & TASAKA, K. 1990 Results of 0.5% Cold Leg Break LOCA experiments at ROSA-IV/LSTF—effect of break orientation. *Expl therm. Fluid Sci.* **3,** 588–596.

ASAKA, H., KUKITA, Y., YONOMOTO T. & TASAKA, K. 1991 Results of 0.5% Hot Leg Break LOCA experiments at ROSA-IV/LSTF—effect of break orientation. in *Nucl. Tech.* To be published.

CROWLEY, C. J. & ROTHE, P. H. 1981 Flow visualization and break mass flow measurements in small break separate effects experiments. EPRI WS-81-201.

DOA, L. T. C. & CARPENTER, J. M. 1980 Experiment data report for LOFT nuclear small-break experiment L3-5/L3-5A. NUREG/CR-1695, EGG-2060.

GLANSDORFF, P. & PRIGOGINE, I. 1977 *Thermodynamic Theory of Structure, Stability and Fluctuations* (in Japanese). Misuzu Shobo, Tokyo.

JOSEPH, D, D., RENARDY, M. & RENARDY, Y. 1984 Instability of the flow of two immiscible liquids with different viscosities in a pipe. *J. Fluid Mech* **141,** 309–317.

LANDAU, L. D. & LIFSHITZ, E. M. 1970 *Fluid Mechanics* (in Japanese). Tokyo Tosho, Tokyo.

LUBIN, B. T. & SPRINGER, G. S. 1967 The formation of a dip on the surface of a liquid draining from a tank. *J. Fluid Mech.* **29,** Part 2, 385–390.

MASIASZEK, T. & MEMPONTEIL, A. 1986 Experimental study on phase separation in a tee junction for steam water stratified inlet flow. *European Two-Phase Flow Group Meeting*, Munich.

MISHIMA, K. & ISHII, M. 1980 Theoretical prediction of onset of horizontal slug flow. *J. Fluids Engng* **102,** 441–445.

REIMANN, J. & KHAN, M. 1983 Flow through a smal break at the bottom of a large pipe with stratified flow. *Int. Topical Meeting on Nuclear Reactor Thermal Hydraulics*, Santa Barbara, U.S.A., pp. 170–177.

SCHROCK, V. E., REVANKAR, S. T., MANNHEIMER, R. & WANG, C. H. 1986 Small break critical discharge—the roles of vapor and liquid entrainment in a stratified two-phase region upstream of the break. NUREG/CR-4761.

SMOGLIE, C. 1984 Two-phase flow through small branches in a horizontal pipe with stratified flow. KfK 3861.

SMOGLIE, C. & REIMANN, J. 1986 Two-phase flow through small branches in a horizontal pipe with stratified flow. *Int. J. Multiphase Flow* **12,** 609–625.

YONOMOTO, T. & TASAKA, K. 1988 New theoretical model for two-phase flow discharged from stratified two-phase region through small break. *J. nucl. Sci. Technol.* **25,** 441–455.

ZUBER, N., 1981 Problems in modeling of small break LOCA. NUREG-0724.

ZIVI, S. M. 1964 Estimation of steady-state steam void-fraction by means of the principle of minimum entropy production. *Trans. ASME Ser. C* **86,** 247–252.

APPENDIX A

Derivation of Basic Equations Used in the Present Model

In the present model, Bernoulli's equation is changed to the following:

$$\tfrac{1}{2}\rho_G v_G^2 = \tfrac{1}{2}\rho_L v_L^2 + \Delta\rho g(h - h_l) \qquad [A.1]$$

where v is velocity and h_l is local water surface level relative to the break. Derivation of [A.1] is shown hereafter.

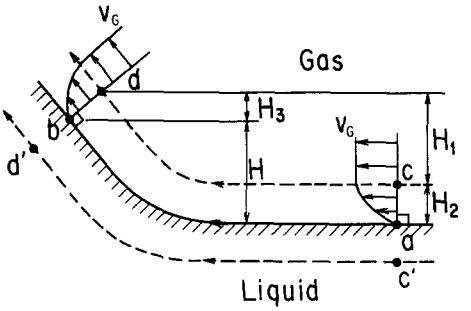

Figure A1. Velocity distribution along the surface.

The fluid velocity is assumed to be the same as the average flow velocity, i.e. the volumetrical flow rate divided by the flow area. By using the assumption of symmetry around the break, the flow area for gas A_G for the top break can be expressed as follows:

$$A_G = \int_0^{\Theta} 2\pi r^2 \cos\theta \, d\theta$$
$$= 2\pi r h_1, \qquad [A.2]$$

where $\Theta = \sin^{-1}(h_1/r)$ (see figure 2 for the meaning of the other symbols). The liquid flow rate is obtained as follows:

$$A_L = 2\pi r(r - h_1) \qquad [A.3]$$

Figure A1 shows the local water surface profile, and the expected velocity profile. Points a and b in the figure are located on the surface, and points c and d are located outside the velocity boundary region in the gas. When points a and c are located very far from the break, the pressure difference between points c and d is expressed as follows:

$$P_c - P_d = [\tfrac{1}{2}\rho_G v_G^2]_d + \rho_G g H_1, \qquad [A.4]$$

(the figure should be referred to for the location of each point and meanings of symbols). The static pressure is considered to be constant in the direction perpendicular to the flow direction. The following relations are therefore derived:

$$P_a - P_c = \rho_G g H_2, \qquad [A.5]$$

$$P_b - P_d = \rho_G g H_3. \qquad [A.6]$$

From [A.4], [A.5] and [A.6], the differential pressure between points a and b is expressed as follows:

$$P_a - P_b = [\tfrac{1}{2}\rho_G v_G^2]_d + \rho_G g H. \qquad [A.7]$$

The same discussion can be applied to the liquid region, which results in:

$$P_a - P_b = [\tfrac{1}{2}\rho_L v_L^2]_d + \rho_L g H. \qquad [A.8]$$

Form [A.7], [A.8] and $H = h - h_1$, the equation [A.1] is obtained.

APPENDIX B

Entrainment Correlation for Side and Bottom Breaks

The present theoretical results are expressed as follows for side and bottom breaks: for the side liquid entrainment,

$$W = \sqrt{2\pi^2 g \rho_G \Delta\rho}\, \frac{\left\{x + (1-x)\sqrt{\dfrac{\rho_G}{\rho_L}}\right\}^2}{\left\{x - (1-x)\sqrt{\dfrac{\rho_G}{\rho_L}}\right\}^2} \frac{h^{2.5}}{x} \quad \text{for} \quad \frac{1}{1+\sqrt{\dfrac{\rho_L}{\rho_G}}} < x < \frac{1}{1+\frac{1}{2}\sqrt{\dfrac{\rho_L}{\rho_G}}},$$

$$W = \frac{\sqrt{2^6\pi^2 g\rho_G \Delta\rho}}{3^{1.5}} \frac{x + (1-x)\sqrt{\frac{\rho_G}{\rho_L}}}{\left\{x - (1-x)\sqrt{\frac{\rho_G}{\rho_L}}\right\}^{2.5}} \sqrt{x} h^{2.5} \quad \text{for} \quad \frac{1}{1+\frac{1}{3}\sqrt{\frac{\rho_L}{\rho_G}}} < x < 1,$$

for the side gas entrainment,

$$W = \sqrt{2\pi^2 g\rho_L \Delta\rho} \frac{\left\{x + (1-x)\sqrt{\frac{\rho_G}{\rho_L}}\right\}^2}{\left\{-x + (1-x)\sqrt{\frac{\rho_G}{\rho_L}}\right\}^2} \frac{h^{2.5}}{1-x} \quad \text{for} \quad \frac{1}{1+3\sqrt{\frac{\rho_L}{\rho_G}}} < x < \frac{1}{1+\sqrt{\frac{\rho_L}{\rho_G}}},$$

$$W = \frac{\sqrt{2^6\pi^2 g\rho_L \Delta\rho}}{3^{1.5}} \frac{1 - x + x\sqrt{\frac{\rho_L}{\rho_G}}}{\left\{1 - x - x\sqrt{\frac{\rho_L}{\rho_G}}\right\}^{2.5}} \sqrt{1-x} h^{2.5} \quad \text{for} \quad 0 < x < \frac{1}{1+3\sqrt{\frac{\rho_L}{\rho_G}}},$$

and for the bottom break,

$$W = \frac{\sqrt{2^5\pi^2 g\rho_L \Delta\rho}}{3^{1.5}} \frac{h^{2.5}}{1-x}\left(1 + \frac{x}{1-x}\sqrt{\frac{\rho_L}{\rho_G}}\right).$$